

Heterogeneous Catalysts Based on Hypercrosslinked Polystyreneand

Subjects: Polymer Science

Contributor: Oleg Manaenkov, Linda Nikoshvili, Alexey Bykov, Olga Kislitsa, Maxim Grigoriev, Mikhail Sulman, Valentina Matveeva, Liubov Kiwi-Minsker

Platform chemicals, also known as chemical building blocks, are substances that serve as starting materials for the synthesis of various value-added products, which find a wide range of applications. These chemicals are the key ingredients for many fine and specialty chemicals. Most of the transformations of platform chemicals are catalytic processes, which should meet the requirements of sustainable chemistry: to be not toxic for humans, to be safe for the environment, and to allow multiple reuses of catalytic materials. Hypercrosslinked polymers are already widely applied in industry as excellent (ad)sorbents. Their use for the synthesis of heterogeneous catalysts is a relatively new but dynamically developing area. A new class of heterogeneous catalysts based on nanoparticles of catalytically active metals stabilized in a polymer matrix of hypercrosslinked polystyrene (HPS) are provided, their synthesis, properties, and application to produce several platform chemicals from renewable raw materials. Some transformations of platform chemicals into compounds with high added value are addressed and multiple perspectives are discussed.

Keywords: porous organic polymer ; hypercrosslinked polystyrene ; platform chemicals ; heterogeneous catalysts ; metal nanoparticles ; biomass processing

1. Hydrolytic Hydrogenation of Cellulose to Hexitols

Sugar alcohols, including sorbitol, are included in the list of substances with high added value obtained from biomass [1]. Sorbitol is a product of glucose hydrogenation and an industrial raw material [2][3]. It is used in the food, textile, pharmaceutical, and cosmetology industries for the synthesis of vitamin C, surfactants, resins, glycols, lactic acid, etc. [4]. The main industrial method for producing sorbitol is the hydrogenation of glucose, which can be obtained from components of plant biomass, like easily hydrolyzed starch or cellulose [6].

Cellulose has no nutritional value and comes in large quantities as a waste from the paper, woodworking, and agricultural industries that require disposal. Therefore, using it as a renewable raw material to produce sorbitol is in accordance with the principles of green chemistry, and can be economically beneficial. The presence of many hydroxyl groups in the structure of cellulose determines one of the most effective options for its processing, namely, conversion into hexitols through the hydrolytic hydrogenation [7][8], known as one-pot reactions of hydrolysis and hydrogenation (**Figure 1**). The products of hydrolytic hydrogenation of cellulose are mainly hexitols (sorbitol and mannitol) and some amounts of C₂–C₅ polyols formed as a result of hydrogenolysis of monosaccharides and polyols.

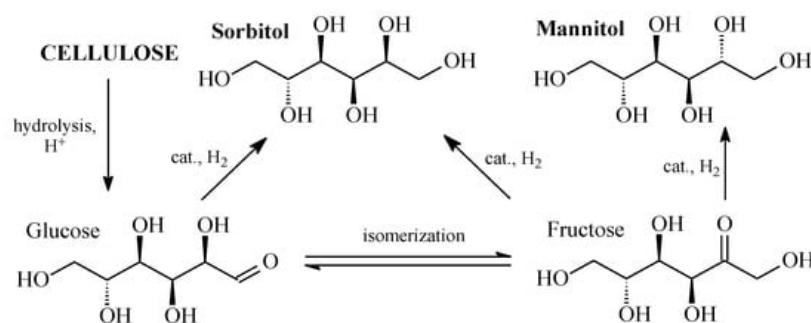


Figure 1. Scheme of hydrolytic hydrogenation of cellulose to hexitols [10].

The study of simultaneous hydrolysis and hydrogenation of plant polysaccharides began in the 1950s by A.A. Balandin et al., who subjected cellulose to hydrolytic hydrogenation in the presence of mineral acids and Ru-, Pd-, and Pt-containing

catalysts [11][12]. For example, in the invention [13] high yield of sorbitol during the hydrolytic hydrogenation of cellulose is claimed in the presence of suspended nickel catalyst at hydrogen pressure of 100–120 atm at 180–200 °C for 40–60 min.

Several decades later, this topic was reconsidered due to the concepts of Green Chemistry [14]. The number of reports on the hydrolytic hydrogenation and hydrogenolysis of cellulose began to increase [15][16]. For environmental reasons, in some cases (under subcritical conditions) the mineral acids as hydrolysis catalysts were replaced by cheap and environmentally friendly water [17][18]. In the late 1990s, Sasaki et al. [19][20] studying the kinetics of dissolution and hydrolysis of cellulose in subcritical and supercritical water showed that in the supercritical region (at a temperature of 374 °C and above) the rate of cellulose hydrolysis is higher than the rate of thermal destruction of glucose, while in subcritical conditions the rate of glucose destruction significantly exceeds the rate of hydrolysis of cellulose macromolecules. Thus, the efficiency of the process of hydrolytic hydrogenation of cellulose carried out in a subcritical water environment will largely be determined by the activity of the catalyst, its ability to quickly and selectively hydrogenate hexoses, which is confirmed by the results of experiments without a catalyst. In the latter case, solutions are formed with an odor and color characteristic of products of the thermal destruction of glucose.

Large numbers of heterogeneous catalytic systems for the direct conversion of cellulose to sorbitol have been proposed. An assessment of the activity of various catalysts in the conversion of biomass into fuel and chemicals showed that catalysts containing noble metals have the highest efficiency [21]. The ruthenium-based catalyst has the maximum activity and comes first in the series: Ru >> Pt ≈ Pd ≈ Au > Rh > Ir >> Os. This is the reason why ruthenium is part of the majority of catalytic systems proposed for the hydrolytic hydrogenation of cellulose and its oligomers with high potential for practical application [22][23][24][25][26][27].

Based on the results obtained in the hydrogenation of mono- and disaccharides with HPS-based catalysts [28][29], our group proposed the use of Ru/HPS catalysts in the hydrolytic hydrogenation of microcrystalline cellulose to produce sorbitol and mannitol [27].

The catalysts were synthesized using the following procedure: HPS was impregnated according to incipient wetness impregnation with the solution of the calculated amount of ruthenium (IV) hydroxochloride in a complex solvent consisting of tetrahydrofuran, methanol, and water at a volume ratio 4:1:1 at room temperature. Then, the catalyst was dried at 70 °C, consecutively treated with solutions of NaOH and H₂O₂, and then washed with water until the absence of chloride anions in the washing water. The catalyst was then dried at 85 °C, reduced by hydrogen at 300 °C and atmospheric pressure for 2 h, cooled in nitrogen and kept under air. The catalyst particle size was controlled by sieving (mesh size 60 μm) the initial powdered support. Commercial sorbents HPS MN270 (without functional groups), MN100 (functionalized with amino groups), and MN500 (functionalized with sulfo groups), were purchased from Purolite, UK, and used for the synthesis.

It was found that the catalyst based on HPS MN270 has the maximum catalytic activity in this process. Its functionalized analogues showed much worse results. Comparing the results of nitrogen physical adsorption, one can see that the 1% Ru/MN500 catalyst during the reduction in hydrogen at 300 °C underwent significant structural changes, leading to a more than fivefold decrease in the specific surface area and a huge decrease in the surface of micropores. This is due to a desulfurization of MN500 at temperatures of 100–150 °C [30] affecting the HPS structure.

HPS MN270 and MN100 are thermostable as confirmed by thermogravimetry results [27]. Intensive, multi-stage (probably associated with the rupture of methylene crosslinks) destruction of HPS MN270 begins at about 450 °C. At this temperature the rate of polymer mass loss attains the maximum of 10%/min. A similar behavior is observed for HPS MN100. Intensive destruction of this polymer also begins around 450 °C. However, the maximum rate of mass loss is higher and attains 15%/min. HPS MN100 degrades faster, probably due to the removal of NH₂ groups. The results obtained suggest that reducing the catalyst based on HPS MN270 and MN100 in hydrogen flow at 300 °C does not affect the HPS morphology.

The main products of hydrolytic hydrogenation of cellulose using a 1% Ru/MN270 catalyst are sorbitol and mannitol; minor products include 1,4-sorbitan, xylitol, erythritol, glycerol, glycols, and some glucose. In addition, trace amounts of glycolic acid, 2-methylpropane-1,2-diol, 3-methylbutane-1,2-diol, butane-1,4-diol, pentane-1,5-diol, hexane-diol, 1,2,6-triol, hexane-1,2,5,6-tetrol, hexane-1,2,3,4,5-pentol, hexane-1,2,3,5,6-pentol, cellobiose, cellotriose, cellotetraose, and other products were found in the reaction medium. The gas phase contains methane and trace amounts of ethane, propane, and isobutane.

Comparing the results obtained with those available in the literature [8][31][32][33][34][35][36][37][38], it should be noted that in the hydrolytic hydrogenation reaction, the 1% Ru/MN270 catalyst showed a fairly high and stable yield of hexitols, a high

degree of cellulose conversion, and its use does not require the pretreatment of cellulose (for example, as in most cases, grinding separately or together with a catalyst) or acid addition to accelerate the hydrolysis of cellulose.

2. Magnetic Catalysts Based on HPS in the Conversion of Plant Polysaccharides

Despite the advantages of homogeneous catalysts, such as high catalytic activity, high selectivity, etc., when creating new industrial catalysts, preference is often given to heterogeneous catalytic systems, which have an important advantage of relatively easy separation from the reaction mixture for subsequent regeneration and reuse [39]. However, existing methods of separation (filtration, centrifugation, decantation, etc.) are laborious, time consuming, and may lead to losses in the catalysts [40], especially if their particles are small in size and density [41]. These problems can be avoided, or at least their impact on production costs can be significantly reduced, if the catalyst particles have magnetic properties [42] [43]. Over the past 10–15 years, a large number of magnetic catalysts have been developed and successfully applied for hydrogenation, oxidation, carbon–carbon coupling, click reactions, Suzuki–Miyaura reactions, chiral and enzyme catalysis, photocatalysis [44][45], in transesterification and esterification reactions for the production of biodiesel fuel [46], etc. Magnetic catalyst separation has the following advantages: fast and efficient separation (the process of separating the catalyst by a magnetic field takes seconds or minutes and the catalyst is completely removed); low energy consumption of separation process (by both a permanent magnet and an electromagnet); the catalyst remains inside the reactor and the process can be quickly restarted with minimal catalyst losses after removing the reaction mixture and introducing a new portion of the substrate into the reactor; magnetic catalysts exhibit their properties only in the presence of a magnetic field and there are thus no additional requirements for the storage, handling, and use of such catalytic systems; sampling and product separation are greatly simplified if the reaction takes place in an inert atmosphere; solvent consumption and waste generation are minimized; the process is easily scaled from laboratory to industrial volumes; and magnetic properties can be imparted to any catalysts (based on enzymes, metals, solid acids, etc.) [40]. Magnetic catalysts are currently being actively developed and have great potential for practical applications in industrial catalytic processes [47]. However, they are not yet used on an industrial scale for a number of reasons. First, the synthesis of magnetic metal and metal oxide nanoparticles often requires expensive precursors and toxic organic solvents, which limits large-scale production [45].

Since HPS has proven to be a suitable catalytic support, we have developed a method for the synthesis of magnetic Ru-containing catalysts based on commercial HPS sorbent MN270 (Purolite, UK). The catalyst was prepared using a two-stage procedure. First, magnetite nanoparticles were synthesized in the pores of HPS through the thermal decomposition of iron (III) acetate. At the second stage, Ru-containing nanoclusters were synthesized on the surface of the composite. To achieve this, the composite powder was impregnated with a solution of ruthenium (IV) hydroxochloride in a complex solvent, dried and kept in hydrogen at 300 °C for 2 h. The resulting magnetic catalysts were tested in the conversion of plant polysaccharides, namely in the process of direct conversion of microcrystalline cellulose into glycols: ethylene glycol (EG) and propylene glycol (PG) [48][49]. EG and PG are the most important raw materials for the production of drugs, fuels, surfactants, antifreezes, lubricants and solvents, lactic acid, etc. [50][51] and in the hydrolytic hydrogenation of inulin to mannitol [52][53].

The process of conversion of cellulose into EG and PG is quite complex (**Figure 2**) and includes several types of reactions, like hydrolysis, isomerization, retro-aldol condensation, hydrogenation, and hydrodeoxygenation [10]. In this regard, development of highly selective catalytic system seems to be rather difficult [54].

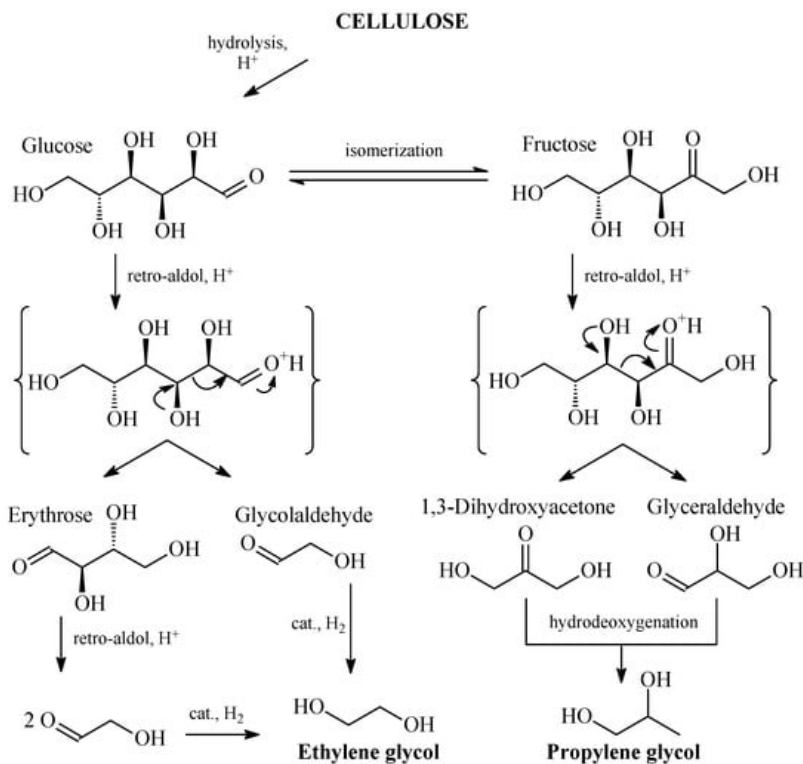


Figure 2. Scheme of the cellulose hydrogenolysis to glycols [10].

The magnetic support ($\text{Fe}_3\text{O}_4/\text{MN270}$) for the Ru-based catalyst was synthesized using the following procedure. FeCl_3 was dissolved in 95% ethanol. HPS powder (diameter < 45 microns) was put into the solution in the ratio of 1 g HPS per 2 g FeCl_3 , mixed thoroughly and left for 10–15 min. Then sodium acetate was added to this mixture in an amount corresponding to the $\text{FeCl}_3/\text{CH}_3\text{COONa}$ ratio of 1/1.5. The mixture was dried until ethanol was completely removed. The resulting red-brown powder was moistened with ethylene glycol, placed in a quartz tube and purged by argon. Then, it was heated up to 300 °C and kept in an argon flow for 5 h. The synthesized $\text{Fe}_3\text{O}_4/\text{MN270}$ powder was washed several times with water, then with ethanol, separated from the solvent with a magnet, and dried to constant weight in an oven at 70 °C in ambient air. The synthesis of 3% Ru- $\text{Fe}_3\text{O}_4/\text{MN270}$ catalyst was carried out using a procedure described in paragraph 4.1 of this review.

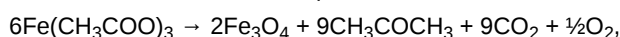
Special attention has been paid to the optimization of magnetite particle formation inside HPS pores. Thus, the use of iron (III) nitrate as a precursor [55], turned out to be harmful for the porous structure of HPS (see **Table 4**). We attributed this result to the formation of strong oxidants during the thermal destruction of nitrate ($4\text{Fe}(\text{NO}_3)_3 \rightarrow 2\text{Fe}_2\text{O}_3 + 12\text{NO}_2 + 3\text{O}_2$). The table data show that the specific surface area of such a sample (Entry 3) is about 50-fold smaller as compared to the sample synthesized using FeCl_3 (Entry 2) as a precursor. It has been shown that the sequential introduction of iron and ruthenium oxides (Entry 4) into the HPS support, the SSA (BET) decreases from 1075 to 364 m^2/g . Although the proportion of pores with a diameter <6 nm decreases slightly, the samples retain their micro/mesoporous character.

Table 4. Porosity data for the HPS and the $\text{Fe}_3\text{O}_4/\text{MN270}$ samples.

Therefore, co-impregnation by iron (III) chloride and CH_3COONa was used for the synthesis of $\text{Fe}_3\text{O}_4/\text{MN270}$ composites. The reactions occurring during the synthesis process can be represented as follows:



As a result of the exchange reaction, $\text{Fe}(\text{CH}_3\text{COO})_3$ is formed in the pores of HPS. It is important to use 95% ethanol as a solvent to prevent hydrolysis of the resulting iron acetate. In the case when hydrolysis does not occur, the subsequent reaction of thermal decomposition of acetate at 300 °C takes place [56]:



During these reactions, a significantly smaller amount of oxygen is formed, which is quickly removed by a flow of inert gas, protecting the polymer pore system.

The synthesized composite was characterized by various methods. First, its magnetic properties were determined and the presence of magnetite nanoparticles with superparamagnetic properties in the pores of HPS was confirmed. **Figure 3** shows the magnetization curves of $\text{Fe}_3\text{O}_4/\text{MN270}$ obtained at 25 °C. The absence of hysteresis in the curves indicates the superparamagnetic nature of the material. In addition, a fairly high saturation magnetization value of 4.0 ± 0.5 emu/g was confirmed, which allows the catalyst to be separated from the reaction mixture quickly and fully.

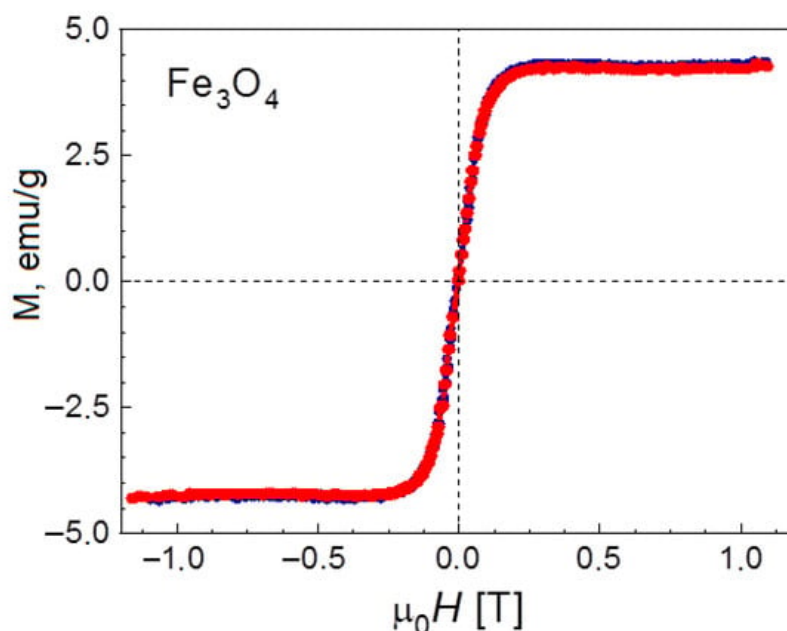


Figure 3. Curves of the $\text{Fe}_3\text{O}_4/\text{MN270}$ sample (red line—magnetization curve; blue line—demagnetization curve) [51].

Powder X-ray diffraction data confirmed the magnetite particles formation. The XRD pattern of $\text{Fe}_3\text{O}_4/\text{MN270}$ displays sharp Bragg reflections whose intensity and positions are typical for magnetite (**Figure 4**).

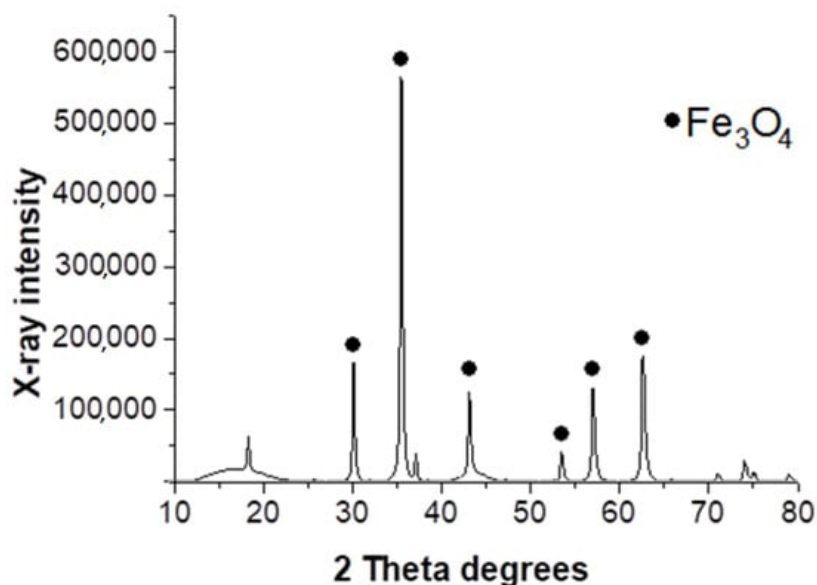


Figure 4. XRD pattern of the $\text{Fe}_3\text{O}_4/\text{MN270}$ [51].

X-ray fluorescence analysis of the 3% Ru- $\text{Fe}_3\text{O}_4/\text{MN270}$ catalyst gave an Fe content of 19.6 wt.%, and a Ru content of 2.7 wt.%.

Based on TEM results, the mean diameter of Ru nanoparticles of 2.0 ± 0.5 nm and magnetite particles of 40 ± 5 nm was determined.

The synthesized catalyst was used in the hydrogenolysis of microcrystalline cellulose under optimal reaction conditions [55]: 255 °C; 60 bar H_2 ; 55 min; 0.3 g of cellulose; 0.07 g of catalyst; 30 mL H_2O ; and 0.195 mol of $\text{Ca}(\text{OH})_2$ per 1 mol of

cellulose.

It was found that the glycol selectivity with the 3% Ru-Fe₃O₄/MN270 magnetic catalyst is approximately equal to the selectivity of 5% Ru-Fe₃O₄-SiO₂ at the same conversion level [55]. However, due to the lower ruthenium content of the HPS catalyst, its specific activity (calculated per gram of Ru) was higher by 35% for EG and 20% for PG.

A comparison of the results for the 3% Ru/MN270 (entry 3) and for the 3% Ru-Fe₃O₄/MN270 catalysts shows that Fe₃O₄ promotes hydrogenolysis, increasing the yield of glycols. According to [57][58], the activity and selectivity of catalytic hydrogenation are significantly improved when catalytic nanoparticles are supported on iron oxide. Moreover, an intimate contact of catalytic and magnetic nanoparticles can lead to electron transfer from the iron oxide to ruthenium surface [59], facilitating hydrogenation [60].

The reuse of the 3% Ru-Fe₃O₄/MN270 catalyst in multiple reaction cycles showed its stability under hydrothermal conditions without any loss of magnetic properties [49]. This is an important advantage for its application in biomass processing, which often is characterized by incomplete conversion of the initial substrates and the formation of large number of byproducts; a separation of the catalyst thus becomes a challenge.

This catalyst was also used for the hydrolytic hydrogenation of inulin, a plant polyfructosan (Figure 5). The high content of inulin in some plants allow this polysaccharide to be a promising renewable source for the production of chemicals and fuel [61]. For example, Jerusalem artichoke (*Helianthus tuberosus* L.) contains up to 82% inulin and has great prospects for cultivation. The main product of the reaction is mannitol, which is used, in particular, in the treatment of brain diseases [62], as a food additive, in perfumery, and for the production of varnishes, resins, surfactants, and other products [63][64].

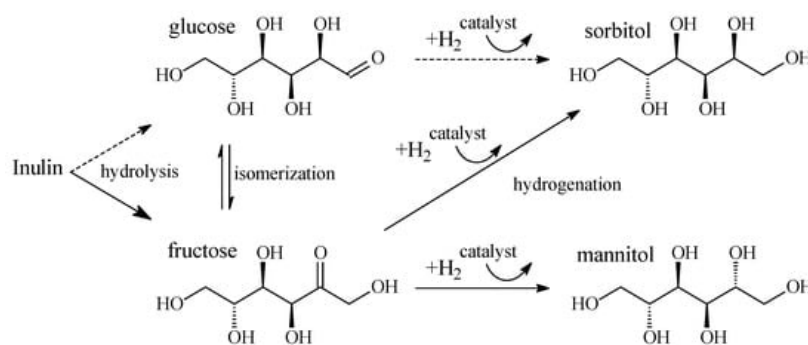


Figure 5. Scheme of the hydrolytic hydrogenation of inulin [10].

Heinen et al. [65] studied the conversion of inulin to mannitol using Ru-containing activated carbon treated with ammonium persulfate as a catalyst. The maximum selectivity for mannitol was 40%. The authors found a certain amount of short-chain inulin oligomers of the GF_n composition (G-glucose, F-fructose) in the solution. The authors explain their presence in the reaction medium after the reaction completion by the fact that the formation of hexitols from inulin occurs simultaneously along two paths: hydrolysis of inulin to monosaccharides with their subsequent hydrogenation and hydrogenation of F_m fragments of inulin with their subsequent hydrolysis. The GF_n fragments formed during the hydrolysis of inulin do not undergo hydrogenation and accumulate in some quantities in the catalyst. In [66], the process of hydrolytic hydrogenation of inulin was studied in the presence of a Ru-containing homogeneous catalyst based on trisulfonated triphenylphosphine ((TPPTS, P(*m*-C₆H₄SO₃Na)₃)—Ru-TPPTS. It was shown that after hydrogenation of the main part of fructose, the hydrogenation of glucose, and, consequently, the formation of sorbitol becomes more pronounced, and the mannitol/sorbitol ratio in the final solution decreases. However, with hydrolytic hydrogenation of inulin, the mannitol/sorbitol ratio is approximately 30% higher than with the hydrogenation of a mixture of glucose and fructose. As a result, the authors concluded that the stereoselectivity of the hydrogenation of D-fructose units in partially hydrolyzed inulin oligomers is higher than in the hydrogenation of pure fructose. In [67], Ru-containing catalysts based on a Cs-substituted tungsten phosphate support (Ru/Cs_xH_{3-x}PW₁₂O₄₀) were proposed for the hydrolytic hydrogenation of cellulose and inulin. The total yield of hexitols (sorbitol and mannitol) during the hydrolytic hydrogenation of inulin was 84%. The authors noted that the new catalyst exhibits high activity, despite the absence of strong internal Brønsted acid sites.

For the first time, magnetic catalysts based on mesoporous silicon dioxide for this process were proposed by our group [68]. Testing a new magnetic catalyst based on HPS in the hydrolytic hydrogenation of inulin to mannitol was carried out under previously determined optimal conditions: 0.1167 mmol Ru per 1 g of inulin; 30 mL H₂O; 150 °C; and P(H₂) 60 bar, 45 min. Inulin conversion was 100% for both catalysts. It can be seen that the selectivity to mannitol for 3% Ru-

Fe₃O₄/MN270 is slightly higher than for the 5% Ru-Fe₃O₄/SiO₂ [68]. However, considering the lower ruthenium content in the polymer catalyst, the productivity of 3% Ru-Fe₃O₄/SiO₂ is almost twice as high.

The 3% Ru-Fe₃O₄/MN270 was stable when reused in the hydrolytic hydrogenation of inulin. It was shown that the selectivity to mannitol and the catalyst activity do not change after three consecutive reactions, demonstrating excellent stability in the inulin-to-mannitol conversion. Magnetic properties of the catalyst allow easy separation from the reaction mixture without any loss.

In general, the results of our study confirm that magnetic catalytic systems based on HPS are promising in the conversion of plant polysaccharides into substances of high added value.

3. Hydrolytic Oxidation of Cellobiose to Glucaric Acid

Glucaric acid is an important platform compound used to produce detergents, polymers, and other valuable products [69][70][71]. The glucaric acid market is constantly growing and should reach USD 1.46 billion by 2027 [72]. Currently, glucaric acid is obtained by chemical oxidation of glucose with nitric acid, which is a non-selective, expensive, and environmentally hazardous process [73]. Another option for the synthesis of glucaric acid is oxidation using heterogeneous catalysts through the stage of formation of gluconic acid. The main disadvantage of the existing methods for producing glucaric acid is the use of mono- and disaccharides as raw materials, which have nutritional value (glucose and sucrose). In this regard, plant biomass, which has no nutritional value, is an ideal raw material for the synthesis of acids [74]. Thaore et al. [75] conducted a feasibility study for the production of pure glucaric acid from corn stover by two methods: homogeneous oxidation of glucose with nitric acid and oxidation of glucose with air in the presence of heterogeneous catalysts. The study showed that both options can be economically feasible for industrial use since the costs per 1 kg of product were 2.91 and 2.53 US dollars for homogeneous and heterogeneous oxidation. However, the process using heterogeneous catalysts has about 22% lower environmental impact. In this case, the main problem is the selection of a stable catalyst, which should present a high yield of glucaric acid.

Previously reported results on the HPS-based catalysts for the oxidation of monosaccharides [28][76] suggested that such catalytic systems can be successively applied for producing aldonic and aldaric acids directly from plant biomass. For this purpose, our group synthesized a series of catalysts based on hypercrosslinked polystyrene MN270 containing Pt, Pd, Au, and Ru. The synthesized catalysts were characterized and tested in the conversion of cellobiose to glucaric acid [77].

The synthesis of these catalysts was carried out according to the method given in paragraph 4.1 of this review. The precursors were ruthenium (IV) hydroxochloride, hydrogen hexachloroplatinate (IV) hydrate, sodium tetrachloropalladate (II), and gold (III) chloride hydrate (pure; OJSC Aurat, Moscow, Russia). Thus, using the appropriate precursors, 3% M/MN270 catalysts were synthesized (M = Pt, Pd, Au, Ru).

The synthesized catalysts were characterized via transmission electron microscopy (TEM). The images and the average diameters of metal clusters were obtained (**Figure 6**). The average size of platinum nanoclusters was 2.8 nm; palladium—3.4 nm; and ruthenium—1.8 nm. The diameter of gold nanoclusters turned out to be approximately an order of magnitude larger, 32.1 nm. It should be noted that nanoparticles of all metals were uniformly distributed within the catalyst volume, and there was no metal crust on the surface of the polymer. We hypothesize that the large size of gold nanoparticles is likely due to the nature of the precursor, interaction with the hydrophobic polymer matrix of the support, and the tendency of gold nanoparticles to aggregate. In our recent work, large gold particles (19.3 ± 8.7 nm) were also obtained using a similar method for the synthesis of the 0.5%-PdAu/HPS-R catalyst [78]. In [79], with a gold content of 1 wt.% in the catalyst, the size of Au-containing nanoparticles was also relatively large (10.9 nm or more). Since our catalyst contains significantly more gold (3 wt.%), the particles formed are larger.

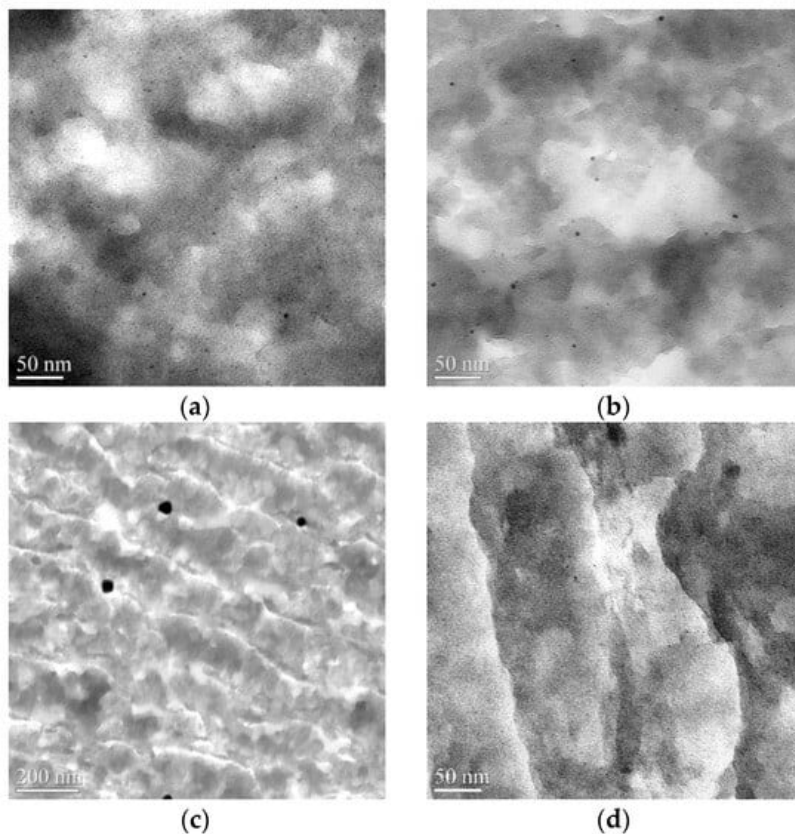


Figure 6. TEM images of catalysts (a) 3% Pt/MN270; (b) 3% Pd/MN270; (c) 3% Au/MN270; (d) 3% Ru/MN270 [77].

The 3% Au/MN270 catalyst was less effective in the cellobiose oxidation reaction. After the end of the experiment, a fairly large amount of glucose and cellobionic acid, as well as a small amount of gluconic acid, were found in the catalyst. Glucaric acid was present in trace quantities. The conversion of cellobiose was 86.2%. The low activity of the Au-containing catalyst could be due to the large particle size of the active phase. Catalysts containing Pd and Ru showed the worst results: low conversion of the initial substrate and extremely low yields of gluconic and glucaric acids. The experiment without a catalyst showed that the catalyst plays the main role in the cellobiose hydrolysis reaction and that the degree of hydrolysis obviously depends on the nature of the metal in the catalyst.

The process conditions were optimized (temperature of 145 °C, an O₂ pressure of 5 bar, and a substrate/catalyst mass ratio of 4/1), and the obtained yields of gluconic and glucaric acids reached 21.6 and 63.4%, respectively, at 100% of cellobiose conversion. The maximum yield of gluconic acid was observed after 1 h of reaction while the maximum yield of glucaric acid was after 2 h.

In the process of the conditions optimization for the hydrolytic oxidation of cellobiose, the obtained qualitative and quantitative results were analyzed and allowed to propose reaction scheme for the conversion of cellobiose into gluconic and glucaric acids in the presence of 3% Pt/MN270 (**Figure 7**).

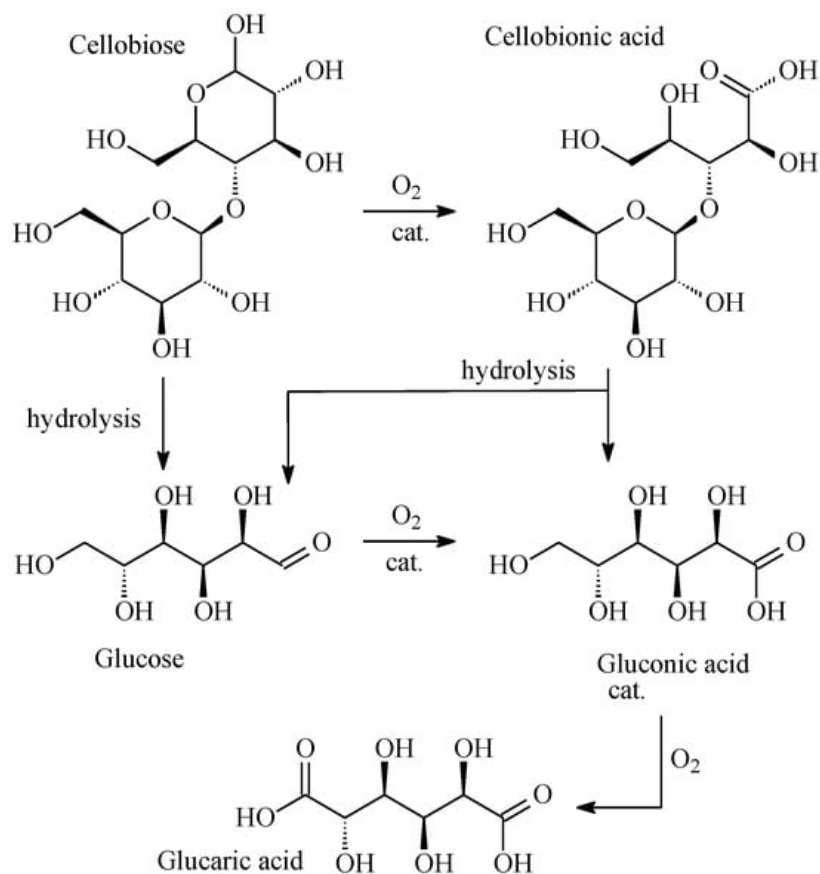


Figure 7. Proposed scheme for the conversion of cellobiose into gluconic and glucaric acids in the presence of the 3% Pt/MN270 catalyst [77].

4. Hydrogenation of Furfural

Technological advances in the field of biomass conversion make it possible to produce a wide range of products of different chemical natures, in particular, furfural (FF), which belongs to the furan group. These compounds are widely used in chemical synthesis because they are highly reactive [80][81]. FF can be produced by sequential hydrolysis and dehydration reactions of xylans that are obtained from biomass. Selective hydrogenation of furfural is important reaction in the production of furfuryl alcohol (FA), methylfuran, tetrahydrofurfuryl alcohol, and other compounds (**Figure 8**).

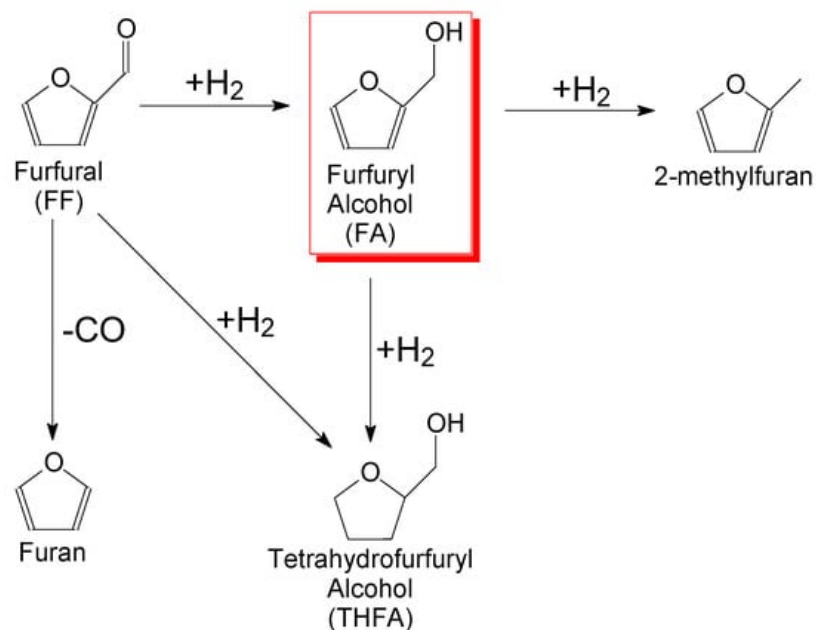


Figure 8. Schematic representation of the FF hydrogenation (the target reaction product is highlighted in red). Reprinted from ref. [82], Copyright 2020, with permission from John Wiley and Sons (Hoboken, New Jersey, USA).

Furfuryl alcohol is mainly used for the production of special resins, lubricants, plasticizers, polymers and the coatings based on them, etc. [83]. Considering that FF hydrogenation is a complex multi-stage process that occurs with the

formation of a large number of products, the synthesis and selection of a suitable catalytic system is very important.

The Pd-containing catalysts based on HPS type MN270 were proposed for the FF hydrogenation. The influence of the precursor nature on the structure, composition, and catalytic properties was studied [84]. Bis(acetonitrile) palladium chloride ($\text{PdCl}_2(\text{CH}_3\text{CN})_2$) and palladium acetate ($\text{Pd}(\text{CH}_3\text{COO})_2$) were used as palladium precursors. All catalysts under study were synthesized via incipient wetness impregnation. The selected Pd (II) precursors have different polarities, which influence their compatibility with HPS and, accordingly, the formation of palladium nanoparticles. The dielectric constants of acetonitrile and acetate are 36.64 and 6.2, respectively [85]. Our previous work [86] showed that HPS is extremely hydrophobic, but due to its unusual porosity and high crosslink density, it can accommodate even completely polar compounds. We believe that the behavior of any compound introduced into a porous matrix depends on its ability to either propagate along the pore walls, when both the matrix and the metal compound have similar properties, or to be repelled from the pore walls (when both are particularly different). This results in particles of different sizes and arrangements depending on the properties of the metal precursor. Therefore, the result depends on the balance of hydrophobicity and hydrophilicity between the metal precursor and HPS [86]. The study using the low-temperature nitrogen physisorption of initial HPS samples and final catalysts showed that the specific surface area of HPS after impregnation with Pd precursors decreased, suggesting pore clogging. It should be noted that the volume of mesopores decreased, while the volume of micropores remained unchanged. These data indicate the formation of palladium nanoparticles in HPS mesopores.

The TEM data (Figure 9) show for the 3% Pd/HPS composite with the $\text{PdCl}_2(\text{CH}_3\text{CN})_2$ precursor, a relatively narrow distribution of Pd nanoparticles with an average diameter of 5.4 ± 1.2 nm (Figure 9a). When using the more hydrophobic precursor $\text{Pd}(\text{CH}_3\text{COO})_2$, a bimodal distribution of particles with average particle sizes of 3.7 ± 1.0 nm and 13.8 ± 5.4 nm is seen (Figure 9b). This observation is consistent with the literature, in that the behavior of metal species in HPS depends on the hydrophobic-hydrophilic balance. The obtained TEM data are also consistent with the BET results, and confirm Pd nanoparticles formation in mesopores rather than micropores.

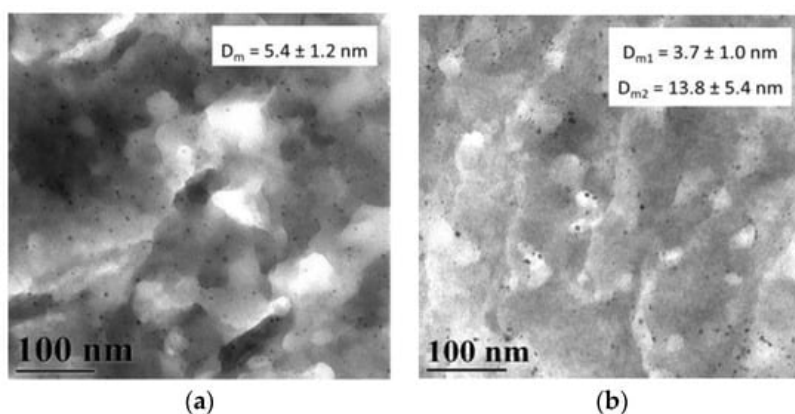


Figure 9. TEM images of the 3% Pd/HPS ($\text{PdCl}_2(\text{CH}_3\text{CN})_2$) (a) and 3% Pd/HPS ($\text{Pd}(\text{CH}_3\text{COO})_2$) (b). Reprinted from ref. [84], Copyright 2019, with permission from Elsevier (Amsterdam, The Netherlands).

The results obtained from small-angle X-ray scattering (SAXS) showed that in the case of 3% Pd/HPS ($\text{PdCl}_2(\text{CH}_3\text{CN})_2$), Pd nanoparticles form a monomodal distribution with an average diameter of 7.5 nm. For the 3% Pd/HPS composite ($\text{Pd}(\text{CH}_3\text{COO})_2$) (b), there are two fractions: a main fraction of small particles (≈ 7 nm) and a small amount of larger particles (10–35 nm) (Figure 10). In general, these results are consistent with the TEM data.

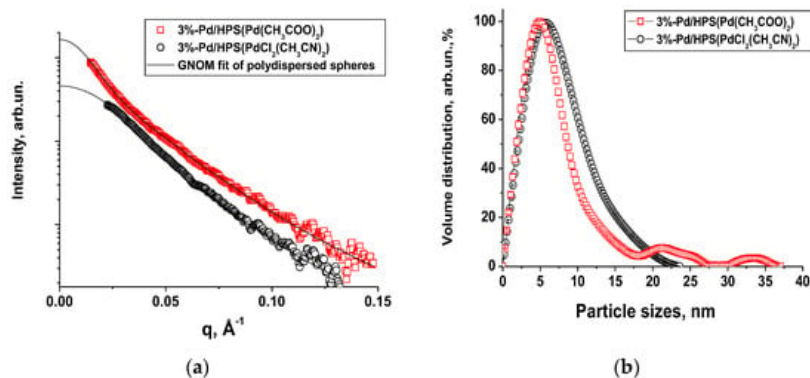


Figure 10. SAXS data for 3% Pd/HPS catalysts after their impregnation with masking liquids (a). Volume particle size distributions of Pd particles in the catalysts (b). Reprinted from ref. [84], Copyright 2019, with permission from Elsevier (Amsterdam, The Netherlands).

XPS data confirm the Pd⁰ nature and oxide form of Pd nanoparticles using both precursors. The XPS spectrum of 3% Pd/HPS(PdCl₂(CH₃CN)₂) is deconvoluted into two components: with Pd 3d_{5/2} binding energies of 335.2 eV and 337.2 eV, which we assign to Pd⁰ (32%) and Pd²⁺ (68%), respectively (**Figure 11**). In the case of 3% Pd/HPS(Pd(CH₃COO)₂) Pd 3d spectrum is also deconvoluted into two components: with Pd 3d_{5/2} binding energies of 335.2 eV (40%) and 336.7 eV (60%) which we also assign to Pd⁰ and Pd²⁺, respectively (**Figure 11**). The typical values of Pd 3d_{5/2} binding energy for Pd⁰ state is about 335.0–335.4 eV and the range of 336–337 eV corresponds to PdO. As the samples were kept on air before XPS study, some part of metal Pd is present in oxide form. The ratio of oxide form/metal form is higher in more disperse samples because small particles are more easily oxidized compared to larger particles. This value could be used to estimate of the ratio between small and large particles in series of such samples. Also, it could be concluded that the nature of Pd precursor in HPS matrix essentially does not influence the Pd oxidation state.

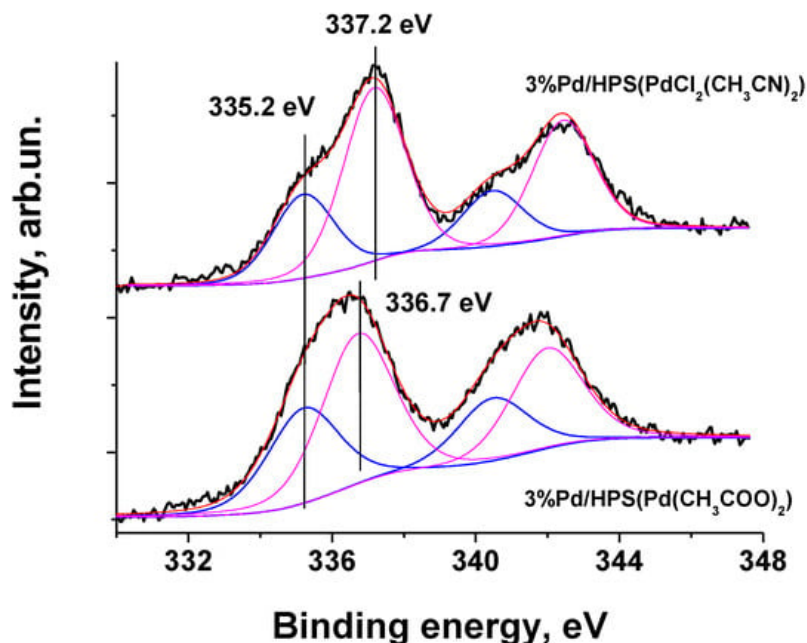


Figure 11. Pd 3d XPS spectra for both Pd/HPS samples and their deconvolution on metal and oxide form of Pd (black line—raw spectrum; red line—synthetic spectrum; blue line—chemical state of palladium Pd⁰; purple line—chemical state of palladium Pd²⁺). Reprinted from ref. [84], Copyright 2019, with permission from Elsevier (Amsterdam, The Netherlands).

A comparison of the catalytic activity of Pd-containing catalysts showed that a more dispersed sample (3% Pd/HPS (PdCl₂(CH₃CN)₂) showed higher values of FF conversion and selectivity towards FA due to the presence of smaller particles catalytically active phase. After 200 min of the reaction, FA selectivity for both catalysts reached its maximum—87.4% for 3% Pd/HPS(PdCl₂(CH₃CN)₂) and 83.8% for the 3% Pd/HPS (Pd(CH₃COO)₂) catalyst at FF conversion of 55.6% and 36.3%, respectively).

Considering good catalytic properties of Pd–Cu alloys in the hydrogenation of FF to FA [87] and the advantages of micro/mesoporous HPS supports in a number of hydrogenation reactions [27][88], we developed new catalysts with Pd–Cu alloy nanoparticles in the pores of HPS and compared their properties with those of monometallic Pd nanoparticles [82]. The catalyst was synthesized by impregnating HPS with a solution containing both palladium and copper acetates, followed by treatment with Na₂CO₃ to precipitate Pd–Cu mixed oxide nanoparticles in the pores of HPS. These as synthesized samples are denoted “as”. The reduction of Pd and Cu species was performed prior to the catalytic reaction in the hydrogen flow at 275 °C. The reduced samples are denoted “r”. SAXS and transmission electron microscopy (TEM) methods were used to estimate the size of nanoparticles (**Figure 12**). The average nanoparticle size determined by using both methods was about 6–7 nm.

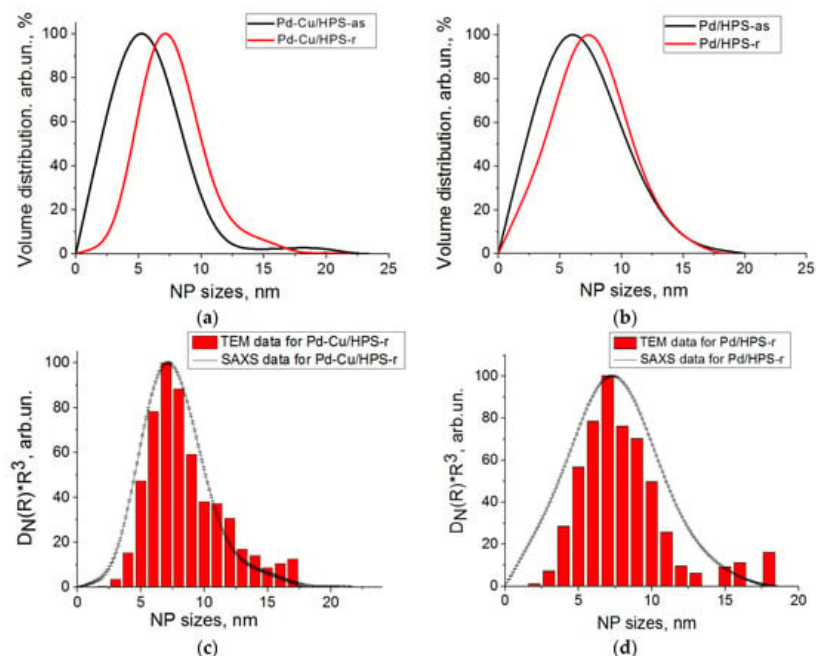


Figure 12. Volume NP size distribution from the SAXS data (a,b), and a comparison of the NP sizes from TEM and SAXS data (c,d) for Pd–Cu/HPS-r (a,c) and Pd/HPS-r (b,d). Reprinted from ref. [82], Copyright 2020, with permission from John Wiley and Sons (Hoboken, New Jersey, USA).

XRD data for Pd/HPS-r shows typical Pd⁰ reflections for a monometallic sample and a crystallite size of 6 nm, indicating that the Pd nanoparticles are most likely single crystals. For bimetallic Pd–Cu nanoparticles in the Pd–Cu/HPS-r sample, the X-ray diffraction pattern is almost identical, but its reflections are shifted towards large angles, and the peak positions are between the positions characteristic of the Pd and Cu phases. According to data from the literature, this peak location indicates the formation of the structure of a Pd–Cu bimetallic alloy. The absence of reflections from Cu metal, as well as its oxides or hydroxides, once again confirms the formation of the alloy. The size of Pd–Cu nanoparticles remains ~6 nm.

XPS showed the enrichment of the surface of nanoparticles with Cu atoms, as well as the presence of both zero-valent and cationic forms of Pd and Cu, i.e., heterogeneity of nanoparticles. This structure of Pd–Cu alloy nanoparticles immobilized in HPS provides almost 100% conversion and excellent selectivity towards FA (95.2%). These exceptional performances were attributed to the prevention of furan ring adsorption on Pd due to neighboring Cu species and facilitated desorption of FA, resulting in higher selectivity. Controlled adsorption of hydrogen and FF due to the mixed valence states of Pd and Cu species leads to higher conversion. These factors, as well as the remarkable ability to reuse the catalyst in ten successive reactions, make this catalyst promising for industrial applications.

5. Hydrogenation of Levulinic Acid

Levulinic acid (LA) is one of the most valuable multifunctional substances obtained from biomass. LA is a precursor to many industrially important chemicals and is widely used in the production of lubricants, chiral reagents, resins, biologically active substances, adsorbents, electronics, and batteries [93][94]. Due to the presence of two highly active functional groups (carbonyl and carboxyl), LA easily enters oxidation, reduction, esterification, substitution, and condensation reactions, which makes it a very valuable platform compound [91]. One of the most important reactions involving LA is hydrogenation to form γ -valerolactone (GVL) (Figure 13), a key reaction in the conversion of plant carbohydrates into renewable fuels and chemicals [92]. GVL can be used as an environmentally friendly solvent, an additive to liquid fuels, and also for the synthesis of polymer precursors such as adipic acid and diols [93][94].

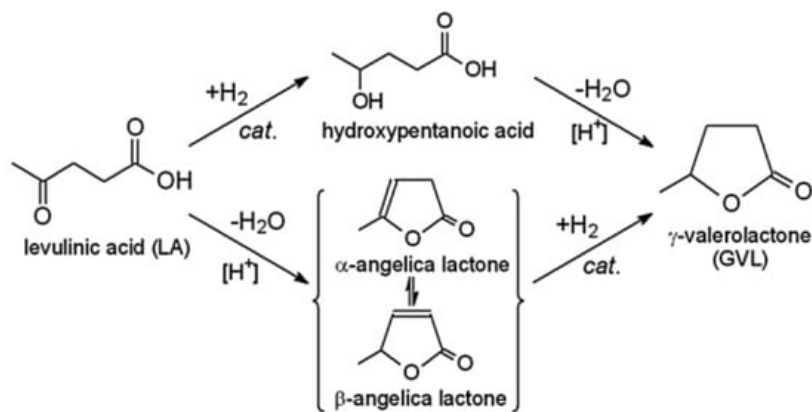


Figure 13. Scheme of LA hydrogenation to GVL. Reprinted from ref. [95], Copyright 2021, with permission from Elsevier (Amsterdam, The Netherlands).

Today, the mostly used in the LA selective hydrogenation to GVL are bifunctional catalysts based on inorganic supports containing Lewis acid sites (LAS) and Brønsted acid sites (BAS). Despite the advantages of bifunctional catalysts in this process, there are some problems caused by the presence of LAS and BAS in the oxide supports. Thus, the high acidity of the support may lead to the formation of coke, which can initiate rapid deactivation of catalysts [96][97][98]. In addition, during the hydrogenation of LA in an aqueous environment, agglomeration and leaching of active metal from the support can occur, which can affect the catalyst stability and significantly complicates its effective reuse [99]. The stability of catalysts can be increased by using carbon supports, which include polymers with a variety of useful properties: high porosity, the presence of functional groups, the ability to vary molecular weight, and hydrophilicity. Balla et al. [100] synthesized uniformly distributed Ni nanoparticles (NPs) with narrow size distribution around 6 nm embedded in a mesoporous carbon substrate (Ni@C) obtained from an organic copolymer. The mesoporous carbon support provided various defect sites for the attachment of Ni particles, and strong interactions between the carbon phase were observed. A total of 100% conversion of LA was achieved in 4 h at 200 °C and 3 MPa in 1,4-dioxane. Balla et al. [101] also synthesized copper NPs (5.5 nm in diameter) embedded in an ordered mesoporous carbon (OMC) carrier by a multicomponent assembly method using chelates. The OMC surface was functionalized with various oxygen-containing functional groups, which enhanced the interaction with copper NPs. The synthesized Cu/OMC catalyst demonstrated high activity and stability in the hydrogenation of LA to GVL in continuous mode (260 °C, 0.1 MPa H₂) due to the effects of Cu retention in mesoporous carbon. Sychev et al. [102] synthesized catalysts based on ruthenium NPs (with a diameter of about 1.5 nm) deposited on the graphite-like mesoporous carbon material Sibunit-4 (initial and oxidized at different temperatures). The presence of oxygen-containing functional groups on the surface of the support was responsible for the distribution of Ru NPs and the acidic properties of the catalyst. The resulting catalysts containing 1% and 3% (wt.) Ru showed high activity in the hydrogenation of LA to GVL (GVL yield 98 mol.% at 160 °C, 1.2 MPa H₂).

References

1. Werpy, T.; Peterson, G. Top Value Added Chemicals from Biomass Volume I—Results of Screening for Potential Candidates from Sugars and Synthesis Gas; National Renewable Energy Laboratory: Golden, CO, USA, 2004; pp. 1–76.
2. Lee, J.; Jung, S.; Kim, Y.T.; Kim, H.J.; Kim, K.-H. Catalytic and electrocatalytic conversion of glucose into value-added chemicals. *Renew. Sust. Energy Rev.* 2023, 181, 113337.
3. Yang, X.; Li, X.; Zhao, J.; Liang, J.; Zhu, J. Production of Sorbitol via Hydrogenation of Glucose over Ruthenium Coordinated with Amino Styrene-co-maleic Anhydride Polymer Encapsulated on Activated Carbon (Ru/ASMA@AC) Catalyst. *Molecules* 2023, 28, 4830.
4. Ahmed, M.J.; Hameed, B.H. Hydrogenation of glucose and fructose into hexitols over heterogeneous catalysts: A review. *J. Taiwan Inst. Chem. Eng.* 2019, 96, 341–352.
5. Newman, A.W.; Vitez, I.M.; Mueller, R.L.; Kiesnowski, C.C.; Findlay, W.P.; Rodriguez, C.; Davidovich, M.; McGeorge, G. Sorbitol. In *Analytical Profiles of Drug Substances and Excipients*; Brittain, H.G., Ed.; Academic Press: Cambridge, MA, USA, 1999; Volume 26, pp. 459–502.
6. Chen, M.; Wang, Y.; Lu, J.; Du, J.; Tao, Y.; Cheng, Y.; Li, Q.; Wang, H. Combinatorial pretreatments of reed straw using liquid hot water and lactic acid for fermentable sugar production. *Fuel* 2023, 331, 125916.

7. Zhang, Y.; Zhang, G.; Chen, T. Efficient one-pot conversion of cellulose to sorbitol over Ni-based carbon. *Fuel* 2023, 339, 127447.
8. Li, Z.Y.; Liu, Y.; Liu, C.F.; Wu, S.B.; Wei, W.Q. Direct conversion of cellulose into sorbitol catalyzed by a bifunctional catalyst. *Bioresour. Technol.* 2019, 274, 190–197.
9. Polidoro, D.; Stamilla, G.; Feltracco, M.; Gambaro, A.; Perosa, A.; Selva, M. CO₂-assisted hydrolytic hydrogenation of cellulose and cellulose-based waste into sorbitol over commercial Ru/C. *Green Chem.* 2023, 25, 6677–6685.
10. Rinaldi, R. *Catalytic Hydrogenation for Biomass Valorization*; RSC Publishing: Cambridge, UK, 2014; 310p.
11. Vasyunina, N.A.; Balandin, A.A.; Chepigo, S.V.; Barysheva, G.S. Catalytic hydrogenation of wood and other vegetable materials. *Bull. Acad. Sci. USSR Div. Chem. Sci.* 1960, 9, 1419.
12. Chepigo, S.V.; Balandin, A.A.; Vasyunina, N.A.; Barysheva, G.S. Preparation of polyhydric alcohols by catalytic transformation of polysaccharides of plant materials. *Chem. Sci. Ind.* 1957, 2, 416–424. (In Russian)
13. Vasyunina, N.A.; Pogosov, Y.L.; Balandin, A.A.; Chepigo, S.V.; Barysheva, G.S. Description of the Invention to Copyright Certificate No. 168666 Method for Producing Polyhydric Alcohols from Cellulose. 1962. (In Russian). Available online: <https://patentdb.ru/image/367900> (accessed on 7 December 2023).
14. Anastas, P.T.; Warner, J.C. *Green Chemistry: Theory and Practice*; Oxford University Press: New York, NY, USA, 2000; 132p.
15. Yang, P.; Kobayashi, H.; Fukuoka, A. Recent Developments in the Catalytic Conversion of Cellulose into Valuable Chemicals. *Chin. J. Catal.* 2011, 32, 716–722.
16. Dhepe, P.L.; Fukuoka, A. Cracking of Cellulose over Supported Metal Catalysts. *Catal. Surv. Asia* 2007, 11, 186–191.
17. Luo, C.; Wang, S.; Liu, H. Cellulose Conversion into Polyols Catalyzed by Reversibly Formed Acids and Supported Ruthenium Clusters in Hot Water. *Ang. Chem. Int. Ed.* 2007, 46, 7636–7639.
18. Shitu, A.; Izhar, S.; Tahir, T.M. Sub-critical water as a green solvent for production of valuable materials from agricultural waste biomass: A review of recent work. *Glob. J. Environ. Sci. Manag.* 2015, 1, 255–264.
19. Sasaki, M.; Kabyemela, B.; Malaluan, R.; Hirose, S.; Takeda, N.; Adschiri, T.; Arai, K. Cellulose hydrolysis in subcritical and supercritical water. *J. Supercrit. Fluid.* 1998, 13, 261–268.
20. Sasaki, M.; Fang, Z.; Fukushima, Y.; Adschiri, T.; Arai, K. Dissolution and Hydrolysis of Cellulose in Subcritical and Supercritical Water. *Ind. Eng. Chem. Res.* 2000, 39, 2883–2890.
21. Makhubela, B.C.E.; Darkwa, J. The Role of Noble Metal Catalysts in Conversion of Biomass and Bio-derived Intermediates to Fuels and Chemicals. *Johns. Matthey Technol. Rev.* 2018, 62, 4–31.
22. Li, Y.; Liao, Y.; Cao, X.; Wang, T.; Ma, L.; Long, J.; Liu, Q.; Xua, Y. Advances in hexitol and ethylene glycol production by one-pot hydrolytic hydrogenation and hydrogenolysis of cellulose. *Biomass Bioenergy* 2015, 74, 148–161.
23. Ribeiro, L.S.; Órfão, J.J.M.; Pereira, M.F.R. Comparative study of different catalysts for the direct conversion of cellulose to sorbitol. *Green Process Synth.* 2015, 4, 71–78.
24. Gromov, N.V.; Medvedeva, T.B.; Rodikova, Y.A.; Timofeeva, M.N.; Panchenko, V.N.; Taran, O.P.; Kozhevnikov, I.V.; Parmon, V.N. One-pot synthesis of sorbitol via hydrolysis-hydrogenation of cellulose in the presence of Ru-containing composites. *Biores. Technol.* 2021, 319, 124122.
25. Carlier, S.; Gripekoven, J.; Philippo, M.; Hermans, S. Ru on N-doped carbon supports for the direct hydrogenation of cellobiose into sorbitol. *Appl. Catal. B Environ.* 2021, 282, 119515.
26. Gromov, N.V.; Medvedeva, T.B.; Taran, O.P.; Timofeeva, M.N.; Said-Aizpuru, O.; Panchenko, V.N.; Gerasimov, E.Y.; Kozhevnikov, I.V.; Parmon, V.N. The main factors affecting the catalytic properties of Ru/Cs-HPA systems in one-pot hydrolysis-hydrogenation of cellulose to sorbitol. *Appl. Catal. A Gen.* 2020, 595, 117489.
27. Matveeva, V.G.; Sulman, E.M.; Manaenkov, O.V.; Filatova, A.E.; Kislitza, O.V.; Sidorov, A.I.; Doluda, V.Y.; Sulman, M.G.; Rebrov, E.V. Hydrolytic hydrogenation of cellulose in subcritical water with the use of the Ru-containing polymeric catalysts. *Catal. Today* 2017, 280, 45–50.
28. Sulman, E.; Doluda, V.; Dzwigaj, S.; Marceau, E.; Kustov, L.; Tkachenko, O.; Bykov, A.; Matveeva, V.; Sulman, M.; Lakina, N. Catalytic properties of Ru nanoparticles introduced in a matrix of hypercrosslinked polystyrene toward the low-temperature oxidation of D-glucose. *J. Mol. Catal. A Chem.* 2007, 278, 112–119.
29. Sapunov, V.N.; Grigoryev, M.Y.; Sulman, E.M.; Konyaeva, M.B.; Matveeva, V.G. D-Glucose hydrogenation over Ru nanoparticles embedded in mesoporous hypercrosslinked polystyrene. *J. Phys. Chem. A* 2013, 117, 4073–4083.
30. Aleksienko, N.N.; Pastukhov, A.V.; Davankov, V.A.; Belyakova, L.D.; Voloshchuk, A.M. Sorption properties of carbonizates of hypercrosslinked polystyrene. *Russ. J. Phys. Chem. A* 2004, 78, 1992–1998.

31. Adsuar-García, M.D.; Flores-Lasluisa, J.X.; Azar, F.Z.; Román-Martínez, M.C. Carbon-Black-Supported Ru Catalysts for the Valorization of Cellulose through Hydrolytic Hydrogenation. *Catalysts* 2018, 8, 572.
32. Rey-Raap, N.; Ribeiro, L.S.; Órfão, J.J.M.; Figueiredo, J.L.; Pereira, M.F.R. Catalytic conversion of cellulose to sorbitol over Ru supported on biomass-derived carbon-based materials. *Appl. Catal. B Environ.* 2019, 256, 117826.
33. Zhang, J.; Wu, S.; Liu, Y. Direct conversion of cellulose into sorbitol over a magnetic catalyst in an extremely low concentration acid system. *Energy Fuels* 2014, 28, 424–4246.
34. Wu, Y.; He, M.; Liu, X.; Wang, X.; Song, Y.; Li, C.; Liu, S.; Huang, L. One-pot Catalytic Conversion of Cellulose to Sorbitol and Isosorbide over Bifunctional Ni/TaOPO₄ Catalysts. *Chemistry Select* 2022, 7, 27 e202200341.
35. Mao, F.; Chen, S.; Zhang, Q.; Yang, L.; Wan, F.; Jiang, D.; Xiong, M.; Zhang, C.; Liu, Y.; Fu, Z. Ru/P-Containing Porous Biochar-Efficiently Catalyzed Cascade Conversion of Cellulose to Sorbitol in Water under Medium-Pressure H₂ Atmosphere. *Bull. Chem. Soc. Jap.* 2020, 93, 1026–1035.
36. Azar, F.-Z.; Lillo-Ródenas, M.Á.; Román-Martínez, M.C. Mesoporous Activated Carbon Supported Ru Catalysts to Efficiently Convert Cellulose into Sorbitol by Hydrolytic Hydrogenation. *Energies* 2020, 13, 4394.
37. Frecha, E.; Remón, J.; Torres, D.; Suelves, I.; Pinilla, J.L. Optimisation of the processing conditions of hydrolytic hydrogenation of cellulose using carbon nanofiber supported Ni catalysts. *Catal. Today* 2023, 423, 114002.
38. Zhang, G.; Chen, T.; Zhang, Y.; Liu, T.; Wang, G. Effective Conversion of Cellulose to Sorbitol Catalyzed by Mesoporous Carbon Supported Ruthenium Combined with Zirconium Phosphate. *Catal. Lett.* 2020, 150, 2294–2303.
39. Ndolomingo, M.J.; Bingwa, N.; Meijboom, R. Review of supported metal nanoparticles: Synthesis methodologies, advantages and application as catalysts. *J. Mater. Sci.* 2020, 55, 6195–6241.
40. Rossi, L.M.; Ferraz, C.P.; Fiorio, J.L.; Vono, L.L.R. Magnetically Recoverable Nanoparticle Catalysts. In *Nanoparticles in Catalysis: Advances in Synthesis and Applications*, 1st ed.; Philippot, K., Roucoux, A., Eds.; WILEY-VCH GmbH: Weinheim, Germany, 2021; pp. 159–181.
41. Goesmann, H.; Feldmann, C. Nanoparticulate functional materials. *Angew. Chem. Int. Ed.* 2010, 49, 1362–1395.
42. Polshettiwar, V.; Luque, R.; Fihri, A.; Zhu, H.; Bouhrara, M.; Basset, J.M. Magnetically recoverable nanocatalysts. *Chem. Rev.* 2011, 111, 3036–3075.
43. Rossi, L.M.; Garcia, M.A.S.; Vono, L.L.R. Recent advances in the development of magnetically recoverable metal nanoparticle catalysts. *J. Braz. Chem. Soc.* 2012, 23, 1959–1971.
44. Rai, P.; Gupta, D. Magnetic nanoparticles as green catalysts in organic synthesis—A review. *Synt. Comm.* 2021, 51, 3059–3083.
45. Zhang, Q.; Yang, X.; Guan, J. Applications of Magnetic Nanomaterials in Heterogeneous Catalysis. *CS Appl. Nano Mater.* 2019, 2, 4681–4697.
46. Xie, W.; Li, J. Magnetic solid catalysts for sustainable and cleaner biodiesel production: A comprehensive review. *Renew. Sust. Energy Rev.* 2023, 171, 113017.
47. Kannapu, H.P.R.; Bathula, H.B.; Suh, Y.-W. Functional magnetic catalysts for the synthesis of biomass-derived fuels and chemicals. In *Advanced Functional Solid Catalysts for Biomass Valorization*, 1st ed.; Hussain, C.M., Sudarsanam, P., Eds.; Elsevier Inc.: Amsterdam, The Netherlands, 2020; pp. 199–223.
48. Manaenkov, O.; Kislitsa, O.; Ratkevich, E.; Matveeva, V.; Sulman, M.; Sulman, E. Ru-Fe₃O₄-containing Polymeric Catalysts for Cellulose Hydrogenolysis. *Chem. Eng. Trans.* 2019, 74, 79–84.
49. Manaenkov, O.; Kosivtsov, Y.; Sapunov, V.; Kislitsa, O.; Sulman, M.; Bykov, A.; Sidorov, A.; Matveeva, V. Kinetic Modeling for the “One-Pot” Hydrogenolysis of Cellulose to Glycols over Ru@Fe₃O₄/Polymer Catalyst. *Reactions* 2022, 3, 1–11.
50. Yue, H.; Zhao, Y.; Ma, X.; Gong, J. Ethylene glycol: Properties, synthesis, and applications. *Crit. Rev. Chem. Soc. Rev.* 2012, 41, 4218–4244.
51. Sugiyama, S.; Tanaka, H.; Bando, T.; Nakagawa, K.; Sotowa, K.-I.; Katou, Y.; Mori, T.; Yasukawa, T.; Ninomiya, W. Liquid-phase oxidation of propylene glycol using heavy-metal-free Pd/C under pressurized oxygen. *Catal. Today* 2013, 203, 116–121.
52. Manaenkov, O.V.; Kislitsa, O.V.; Matveeva, V.G.; Kosivtsov, Y.Y.; Sulman, M.G. Kinetics of the hydrolytic hydrogenation of inulin to mannitol on Ru-containing magnetic catalyst. *ChemChemTech* 2023, 66, 70–76.
53. Sulman, E.; Manaenkov, O.; Kislitsa, O.; Ratkevich, E.; Sulman, M.; Matveeva, V. Magnetically Recoverable Catalysts for Cellulose and Inulin Conversion. *Chem. Eng. Trans.* 2020, 81, 1153–1158.

54. Zheng, M.; Pang, J.; Sun, R.; Wang, A.; Zhang, T. Selectivity Control for Cellulose to Diols: Dancing on Eggs. *ACS Catal.* 2017, 7, 1939–1954.
55. Manaenkov, O.; Mann, J.; Kislitza, O.; Losovyj, Y.; Stein, B.; Morgan, D.; Pink, M.; Lependina, O.; Shifrina, Z.; Matveeva, V.; et al. Ru-containing Magnetically Recoverable Catalysts: A Sustainable Pathway from Cellulose to Ethylene and Propylene Glycols. *ACS Appl. Mater. Interfaces* 2016, 8, 21285–21293.
56. Laurikėnas, A.; Barkauskas, J.; Reklaitis, J.; Niaura, G.; Baltrūnas, D.; Kareiva, A. Formation peculiarities of iron (III) acetate: Potential precursor for iron metal-organic frameworks (MOFs). *Lith. J. Phys.* 2016, 56, 35–41.
57. Musolino, M.G.; Scarpino, L.A.; Mauriello, F.; Pietropaolo, R. Glycerol Hydrogenolysis Promoted by Supported Palladium Catalysts. *ChemSusChem* 2011, 4, 1143–1150.
58. Gumina, G.; Easterday, R.; Malyutin, A.G.; Budgin, A.M.; Stein, B.D.; Nikoshvili, L.Z.; Matveeva, V.G.; Sulman, E.M.; Morgan, D.G.; Bronstein, L.M. γ -Fe₂O₃ Nanoparticle Surface Controls PtFe Nanoparticle Growth and Catalytic Properties. *Nanoscale* 2013, 5, 2921–2927.
59. Easterday, R.; Sanchez-Felix, O.; Losovyj, Y.; Pink, M.; Stein, B.D.; Morgan, D.G.; Rakitin, M.; Doluda, V.Y.; Sulman, M.; Mahmoud, W.E.; et al. Design of Ruthenium/Iron Oxide Nanoparticle Mixtures for Hydrogenation of Nitrobenzene to Aniline: Catalytic Behavior Influenced by Iron Oxide Nanoparticles. *Catal. Sci. Technol.* 2015, 5, 1902–1910.
60. Milone, C.; Crisafulli, C.; Ingoglia, R.; Schipilliti, L.; Galvagno, S. A Comparative Study on the Selective Hydrogenation of Alpha, Beta Unsaturated Aldehyde and Ketone to Unsaturated Alcohols on Au Supported Catalysts. *Catal. Today* 2007, 122, 341–351.
61. Johansson, E.; Prade, T.; Angelidaki, I.; Svensson, S.-E.; Newson, W.R.; Gunnarsson, I.B.; Hovmalm, H.P. Economically Viable Components from Jerusalem Artichoke (*Helianthus tuberosus* L.) in a Biorefinery Concept. *Int. J. Mol. Sci.* 2015, 16, 8997–9016.
62. Gu, J.; Huang, H.; Huang, Y.; Sun, H.; Xu, H. Hypertonic saline or mannitol for treating elevated intracranial pressure in traumatic brain injury: A meta-analysis of randomized controlled trials. *Neurosurg. Rev.* 2019, 42, 499–509.
63. Imhof, P.J.; Van der Waal, J.C. (Eds.) *Catalytic Process Development for Renewable Materials*; WILEY-VCH GmbH: Weinheim, Germany, 2013.
64. Ohrem, H.L.; Schornick, E.; Kalivoda, A.; Ognibene, R. Why is mannitol becoming more and more popular as a pharmaceutical excipient in solid dosage forms? *Pharmaceut. Dev. Technol.* 2014, 19, 257–262.
65. Heinen, A.W.; Peters, J.A.; van Bekkum, H. The combined hydrolysis and hydrogenation of inulin catalyzed by bifunctional Ru/C. *Carbohydr. Res.* 2001, 330, 381–390.
66. Heinen, A.W.; Papadogianakis, G.; Sheldon, R.A.; Peters, J.A.; van Bekkum, H. Factors effecting the hydrogenation of fructose with a water soluble Ru–TPPTS complex. A comparison between homogeneous and heterogeneous catalysis. *J. Mol. Catal. A Chem.* 1999, 142, 17–26.
67. Deng, W.; Zhu, E.; Liu, M.; Zhang, Q.; Wang, Y. Cs-substituted tungstophosphate-supported ruthenium nanoparticles as efficient and robust bifunctional catalysts for the conversion of inulin and cellulose into hexitols in water in the presence of H₂. *RSC Adv.* 2014, 4, 43131–43141.
68. Manaenkov, O.V.; Ratkevich, E.A.; Kislitsa, O.V.; Lawson, B.; Morgan, D.G.; Stepacheva, A.A.; Matveeva, V.G.; Sulman, M.G.; Sulman, E.M.; Bronstein, L.M. Magnetically recoverable catalysts for the conversion of inulin to mannitol. *Energy* 2018, 154, 1–6.
69. Grand view Research, Glucaric Acid Market Size, Share & Trends Analysis by Product (Pure Glucaric Acid, D-Glucaric Acid-1,4-lactone), by Application (Food Ingredients, Detergents, Corrosion Inhibitors), & Segment Forecasts, 2017–2025. Available online: <https://www.grandviewresearch.com/industry-analysis/glucaric-acid-market> (accessed on 14 October 2023).
70. Wu, Y.; Enomoto-Rogers, Y.; Masaki, H.; Iwata, T. Synthesis of crystalline and amphiphilic polymers from D-glucaric acid. *ACS Sustain. Chem. Eng.* 2016, 4, 3812–3819.
71. Mehtio, T.; Toivari, M.; Wiebe, M.G.; Harlin, A.; Penttilä, M.; Koivula, A. Production and applications of carbohydrate-derived sugar acids as generic biobased chemicals. *Crit. Rev. Biotechnol.* 2016, 36, 904–916.
72. Reports and Data. Available online: <https://www.globenewswire.com/news-release/2020/08/24/2082896/0/en/Glucaric-Acid-Market-To-Reach-USD-1-46-Billion-By-2027-Reports-and-Data.html> (accessed on 14 October 2023).
73. Smith, T.N.; Hash, K.; Davey, C.-L.; Mills, H.; Williams, H.; Kiely, D.E. Modifications in the nitric acid oxidation of D-glucose. *Carbohydr. Res.* 2012, 350, 6–13.
74. Sakuta, R.; Nakamura, N. Production of Hexaric Acids from Biomass. *Int. J. Mol. Sci.* 2019, 20, 3660.

75. Thaore, V.B.; Armstrong, R.D.; Hutchings, G.J.; Knight, D.W.; Chadwick, D.; Shah, N. Sustainable production of glucaric acid from corn stover via glucose oxidation: An assessment of homogeneous and heterogeneous catalytic oxidation production routes. *Chem. Eng. Res. Des.* 2020, 153, 337–349.
76. Sidorov, S.N.; Volkov, I.V.; Davankov, V.A.; Tsyurupa, M.P.; Valetsky, P.M.; Bronstein, L.M.; Karlinsey, R.; Zwanziger, J.W.; Matveeva, V.G.; Sulman, E.M.; et al. Platinum-Containing HyperCross-Linked Polystyrene as a Modifier-Free Selective Catalyst for L-Sorbose Oxidation. *J. Am. Chem. Soc.* 2001, 123, 10502–10510.
77. Manaenkov, O.; Kislitsa, O.; Ratkevich, E.; Kosivtsov, Y.; Sapunov, V.; Matveeva, V. Hydrolytic Oxidation of Cellobiose Using Catalysts Containing Noble Metals. *Reactions* 2022, 3, 589–601.
78. Nikoshvili, L.Z.; Shkerina, K.N.; Bykov, A.V.; Sidorov, A.I.; Vasiliev, A.L.; Sulman, M.G.; Kiwi-Minsker, L. Mono- and Bimetallic Nanoparticles Stabilized by an Aromatic Polymeric Network for a Suzuki Cross-Coupling Reaction. *Nanomaterials* 2022, 12, 94.
79. Morawa Eblagon, K.; Pereira, M.F.R.; Figueiredo, J.L. One-pot oxidation of cellobiose to gluconic acid. Unprecedented high selectivity on bifunctional gold catalysts over mesoporous carbon by integrated texture and surface chemistry optimization. *Appl. Catal. B Environ.* 2016, 184, 381–396.
80. Santos Viana, G.; Estevam Lau Bomfim, J.A.; Pereira da Silva, G.; Souza de Carvalho Filho, J.F.; Sanae Tokumoto, M.; Cesário Rangel, F.; Serpa da Cruz, R. Design of Heterogeneous Catalysts for the Conversion of Furfural to C5 Derivatives: A Brief Review. *Catal. Res.* 2022, 2, 026.
81. Racha, A.; Samanta, C.; Sreekantan, S.; Marimuthu, B. Review on Catalytic Hydrogenation of Biomass-Derived Furfural to Furfuryl Alcohol: Recent Advances and Future Trends. *Energy Fuels* 2023, 37, 11475–11496.
82. Salnikova, K.E.; Larichev, Y.V.; Sulman, E.M.; Bykov, A.V.; Sidorov, A.I.; Demidenko, G.N.; Sulman, M.G.; Bronstein, L.M.; Matveeva, V.G. Selective Hydrogenation of Biomass-Derived Furfural: Enhanced Catalytic Performance of Pd-Cu Alloy Nanoparticles in Porous Polymer. *ChemPlusChem.* 2020, 85, 1697–1703.
83. Jorqueira, D.S.S.; de Lima, L.F.; Moya, S.F.; Vilcoq, L.; Richard, D.; Fraga, M.A.; Suppino, R.S. Critical review of furfural and furfuryl alcohol production: Past, present, and future on heterogeneous catalysis. *Appl. Catal. A Gen.* 2023, 665, 119360.
84. Salnikova, K.E.; Matveeva, V.G.; Larichev, Y.V.; Bykov, A.V.; Demidenko, G.N.; Shkileva, I.P.; Sulman, M.G. The liquid phase catalytic hydrogenation of furfural to furfuryl alcohol. *Catal. Today* 2019, 329, 142–148.
85. Lide, D.R. (Ed.) *CRC Handbook of Chemistry and Physics: A Ready-Reference Book of Chemical and Physical Data*; CRC Press: Boca Raton, FL, USA, 1999.
86. Tsvetkova, I.B.; Matveeva, V.G.; Doluda, V.Y.; Bykov, A.V.; Sidorov, A.I.; Schennikov, S.V.; Sulman, M.G.; Valetsky, P.M.; Stein, B.D.; Chen, C.-H.; et al. Pd(II) nanoparticles in porous polystyrene: Factors influencing the nanoparticle size and catalytic properties. *J. Mater. Chem.* 2012, 22, 6441–6448.
87. Liu, P.; Qiu, W.; Zhang, C.; Tan, Q.; Zhang, C.; Zhang, W.; Song, Y.; Wang, H.; Li, C. Kinetics of Furfural Hydrogenation over Bimetallic Overlayer Catalysts and the Effect of Oxygen Vacancy Concentration on Product Selectivity. *ChemCatChem* 2019, 11, 3296–3306.
88. Liu, Q.; Xia, B.; Huang, J.; Liao, B.; Liu, H.; Ou, B.; Chen, L.; Zhou, Z. Hypercrosslinked polystyrene microspheres with ultrahigh surface area and their application in gas storage. *Mater. Chem. Phys.* 2017, 199, 616–622.
89. Kohli, K.; Prajapati, R.; Sharma, B.K. Bio-Based Chemicals from Renewable Biomass for Integrated Biorefineries. *Energies* 2019, 12, 233.
90. Kislitsa, O.V.; Manaenkov, O.V.; Ratkevich, E.A.; Sulman, M.G.; Kosivtsov, Y.Y. The Use of WO₃-ZSM-5 Zeolites in the Dehydration of Monosaccharides. *Chem. Eng. Trans.* 2021, 88, 295–300.
91. Lopes, E.S.; Gariboti, J.C.J.; Feistel, L.; Rivera, E.C.; Maciel Filho, R.; Tovar, L.P. Acid Hydrolysis-based Sugarcane Bagasse Biorefining for Levulinic Acid Production: Dynamic Mechanistic Modeling Under Varying Operating Conditions. *Chem. Eng. Trans.* 2020, 80, 217–222.
92. Huang, X.; Liu, K.; Vrijbur, W.L.; Ouyang, X.; Iulian Dugulan, A.; Liu, Y.; Tiny Verhoeven, M.W.G.M.; Kosinov, N.A.; Pidko, E.A.; Hensen, E.J.M. Hydrogenation of Levulinic Acid to γ -Valerolactone over Fe-Re/TiO₂ Catalysts. *Appl. Catal. B Environ.* 2020, 278, 119314.
93. Genuino, H.C.; van de Bovenkamp, H.H.; Wilbers, E.; Winkelmann, J.G.M.; Goryachev, A.; Hofmann, J.P.; Hensen, E.J.M.; Weckhuysen, B.M.; Bruijninx, P.C.A.; Heeres, H.J. Catalytic Hydrogenation of Renewable Levulinic Acid to γ -Valerolactone: Insights into the Influence of Feed Impurities on Catalyst Performance in Batch and Flow Reactors. *ACS Sustain. Chem. Eng.* 2020, 8, 5903–5919.
94. Li, W.; Li, F.; Chen, J.; Betancourt, L.E.; Tu, C.; Liao, M.; Ning, X.; Zheng, J.; Li, R. Efficient and sustainable hydrogenation of levulinic acid to γ -valerolactone in aqueous phase over Ru/MCM-49 catalysts. *Ind. Eng. Chem.*

Res. 2020, 59, 17338–17347.

95. Grigorev, M.E.; Mikhailov, S.P.; Bykov, A.V.; Sidorov, A.I.; Tiamina, I.Y.; Vasiliev, A.L.; Nikoshvili, L.Z.; Matveeva, V.G.; Plentz Meneghetti, S.M.; Sulman, M.G.; et al. Mono- and bimetallic (Ru-Co) polymeric catalysts for levulinic acid hydrogenation. *Catal. Today* 2021, 378, 167–175.
96. Luo, W.; Deka, U.; Beale, A.M.; van Eck, E.R.H.; Bruijninx, P.C.A.; Weckhuysen, B.M. Ruthenium-catalyzed hydrogenation of levulinic acid: Influence of the support and solvent on catalyst selectivity and stability. *J. Catal.* 2013, 301, 175–186.
97. Yu, Z.; Lu, X.; Xiong, J.; Ji, N. Transformation of Levulinic Acid to Valeric Biofuels: A Review on Heterogeneous Bifunctional Catalytic Systems. *ChemSusChem* 2019, 6, 3915–3930.
98. Amarasekara, A.S.; Wiredu, B.; Grady, T.L.; Obregon, R.G.; Margetic, D. Solid acid catalyzed aldol dimerization of levulinic acid for the preparation of C10 renewable fuel and chemical feedstocks. *Catal. Commun.* 2019, 124, 6–11.
99. Sun, P.; Gao, G.; Zhao, Z.; Xia, C.; Li, F. Acidity-regulation for enhancing the stability of Ni/HZSM-5 catalyst for valeric biofuel production. *Appl. Catal. B Environ.* 2016, 189, 19–25.
100. Balla, P.; Seelam, P.K.; Balaga, R.; Rajesh, R.; Perupogu, V.; Liang, T.X. Immobilized highly dispersed Ni nanoparticles over porous carbon as an efficient catalyst for selective hydrogenation of furfural and levulinic acid. *J. Environ. Chem. Eng.* 2021, 9, 106530.
101. Balla, P.; Seelam, P.K.; Rajesh, R.; Balaga, R.; Challa, P.; Sasikumar, G.K.; Perupogu, V.; Lassi, U.; Sungtak, K. Selective hydrogenation of levulinic acid over a highly dispersed and stable copper particles embedded into the ordered mesoporous carbon supported catalyst. *Catal. Com.* 2023, 178, 106673.
102. Sychev, V.V.; Baryshnikov, S.V.; Ivanov, I.P.; Volochaev, M.N.; Taran, O.P. Hydrogenation of levulinic acid to γ -valerolactone in the presence of Ru-containing catalysts based on carbon material “Sibunit”. *J. Sib. Fed. Univ. Chem.* 2021, 14, 5–20.

Retrieved from <https://encyclopedia.pub/entry/history/show/120501>